Electrochemistry
The Electrochemical Society of Japan
Received: May 26, 2020
Accepted: June 15, 2020
Published online: July 31, 2020
https://doi.org/10.5796/electrochemistry.20-64066
Article
Electrochemistry, **88(5)**, 380–386 (2020)

The 64th special issue "Frontiers of Carbon Materials"

Study on Fabrication and Electrochemical Performances of Fe_7S_8@C Composite Materials

Jianke LI,[a] Guiying XU,[a,*] Kun WANG,[b] Beibei HAN,[c] Lixiang LI,[a] Yingxin WANG,[d] Dongying JU,[b,c] Maorong CHAI,[c] Dakui ZHANG,[e] and WeiMin ZHOU[a,*]

[a] *Key Laboratory of Energy Materials and Electrochemistry Research Liaoning Province, University of Science and Technology Liaoning, Anshan 114051, P. R. China*
[b] *School of Materials and Metallurgy, University of Science and Technology Liaoning, Anshan 114051, P. R. China*
[c] *Advanced Science Research Laboratory, Saitama Institute of Technology, 1690 Fusaiji, Fukaya, Japan*
[d] *JiXi Weida New Material Technology Co., Ltd., No. 8, Lexin Street, Jiguan Industrial Park, Jixi City, Heilongjiang Province, China*
[e] *Ansteel Chemical Co., Ltd., No. 1 Huangang Road, Tiexi District, Anshan City, Liaoning Province, China*

* *Corresponding author: aszhou15242870697@163.com*

ABSTRACT

Fe_7S_8@C composite materials are facilely fabricated using the gelatin, $FeSO_4{\cdot}7H_2O$ and $Na_2S{\cdot}9H_2O$ by one-step method. The obtained Fe_7S_8@C composite materials show the fabulous rate performances and cycling performances, when controlling the carbon contents in Fe_7S_8@C composite materials. For instance, the Fe_7S_8@C-40 shows the cycling performance at 657.3 mAh/g, after carrying out the charge-discharge cycles 400 times. These electrochemical performances lead us to consider our provided preparation method is the effective way to facilitate the application of Fe_7S_8@C in fabrication of lithium ion batteries (LIBs) as negative electrode materials.

Keywords : Fe_7S_8 Compound, Metal Sulfides, Lithium Ion Batteries (LIBs), Fe_7S_8@C Composite Materials

1. Introduction

Lithium ion batteries (LIBs) are significantly intrigued by now, compared with other energy storage materials. It is acknowledged that graphite as general negative electrode materials are widely used to fabricate LIBs. However, the relatively low charge efficiency and energy density of graphitized carbons limit their actual applications as negative electrode materials.[1,2] The concept that carbon mixes the active materials is extensively utilized to fabricate electrode materials.[3–9] In particular, transition metal oxides such as Fe_2O_3, Fe_3O_4, FeO are entering the visions of researches, for they have the high theoretical capacity.[10–13] Thus, the composite method using the metal oxides with carbon materials is becoming popular gradually.

On the other hand, metal sulfides are attracted than ever before, for they possess the attractive physical and chemical properties such as outstanding mechanical stability, thermal stability and advantageous oxidation-reduction reaction and so on. In particular, the Fe_7S_8 has been attracted gradually, for the mixed-valence of Fe_7S_8 leads it owns the relatively tremendous conductivity.[14,15] Nevertheless, similar to general metal oxides, the phenomenon of volume expansion also exists in metal sulfides. Meanwhile, the slow Li^+ transfer in metal sulfide lattice restricts the enhancing of storage capacity.[16] Therefore, how to solve the above problem of metal sulfides is becoming hot research topic rapidly.

To date, a lot of researches indicate that covering the carbon materials on the surface of metal oxide is able to improve the conductivity and Li^+ transfer not only, but also can solve the troublesome problem of volume expansion.[17,18] Likewise, Fe_7S_8@C composite materials having the tremendous Li^+ and Na^+ storage capacity were fabricated using the Fe_2O_3, poly(dopamine) (PDA) and thioacetamide (TAA). This report points out Fe_7S_8@C materials possess high possibility in application as negative electrode materials.[19]

To expand the application of Fe_7S_8@C as negative electrode materials, we explore the more facile method to prepare the Fe_7S_8@C materials. In our studies, we pour attention to the gelatin, for it has a number of organic groups which can remarkably facilitate the metal oxide compounds disperse in it.[20] Consequently, we used the gelatin as carbon source, $FeSO_4{\cdot}7H_2O$ as iron source and $Na_2S{\cdot}9H_2O$ as sulfur source to fabricate the Fe_7S_8@C composite materials by one-step method. As a result, the prepared Fe_7S_8@C materials exhibit the superior dispersing property of Fe_7S_8 with nanometer size and applicable electrochemical performances.

2. Experimental

2.1 Characterization

The measurements of X-ray diffraction (XRD) were carried out by X'pert Powder instrument from PANalytical, Holland. SEM morphologies were evaluated by instrument of Carl Zeiss AG, Germany. Thermogravimetric analysis (TGA) was performed by thermal gravimetric analyzer (TG209F3) of NETZSCH Group, Germany. The X-ray photoelectron spectroscopy (XPS) measurements were carried out by Axis Ultra DLD instrument of Kratos, UK. Nitrogen adsorption and desorption isotherm was measured by Quadrasorb autosorb-iQ surface analyzer which was purchased from Quantachrome Instruments, USA. Specific surface area was determined in detail, according to the BET method. The pore size distribution was assessed by DFT model for slit pores. Electrochemical measurements were performed by the electrochemical system (CHI660E) of ChenHua, Shanghai, China. Table type high speed centrifuge was purchased from Shanghai Fichal Analytical Instrument Co., Ltd., China. Transmission Electron Microscope

(TEM) measurements were carried out by the HF-3300 Hitachi, Ltd., Japan.

2.2 Preparation of Fe_7S_8 compound

The Fe_7S_8 was prepared successfully, referring to the lecture reported by Mu et al.[21] Specifically, the $FeSO_4{\cdot}7H_2O$ (5.56 g) and $Na_2S{\cdot}9H_2O$ (4.80 g) were dissolved in the deionized water (80 mL) respectively. The solution containing the $Na_2S{\cdot}9H_2O$ was slowly added into the solution containing the $FeSO_4{\cdot}7H_2O$, and the obtained mixture solution was stirred for 5 min at 60 °C. After filtering the reacted mixture, the black solid was obtained and continuously carried out the vacuum drying process at 80 °C for 24 h. Finally, the Fe_7S_8 solids were obtained, after they had been washed and dried completely.

2.3 Preparations of Fe_7S_8@C composite materials

Firstly, the gelatin (10 g) was dissolved in the deionized water (90 mL) at 85 °C, and the obtained solution was uniformly stirred with the 300 r/min. As a result, the gelatin solution with light yellow color was obtained and named ***α***. Thereafter, the $FeSO_4{\cdot}7H_2O$ (5.56 g) and $Na_2S{\cdot}9H_2O$ (4.80 g) were dissolved in the deionized water (80 mL) respectively, and the obtained solutions were named as ***β*** and ***γ*** solutions. Continuously, the ***β*** solution was respectively added to the ***α*** solutions owning the volumes of 30 mL, 40 mL and 50 mL, and the obtained mixture solutions were homogeneously stirred at 60 °C. After the obtained three kinds of mixture solutions were respectively mixed with the same ***γ*** solution, the obtained new mixture solutions were stirred for 1 h at 60 °C. The obtained final mixture solutions were placed in the oven at 80 °C for 24 h, and continuously treated at 500 °C for 4 h. After cooling the obtained solids to the room temperature, the products were washed by the deionized water many times and dried entirely. Finally, according to the usage of volumes of gelatin solutions (***α***), the obtained composite solids were named as Fe_7S_8@C-30, Fe_7S_8@C-40 and Fe_7S_8@C-50, respectively.

2.4 Electrochemical measurements

The electrochemical cells were prepared using the Fe_7S_8@C composite materials. Firstly, Fe_7S_8@C composite materials (0.08 g) were respectively mixed with acetylene black (0.01 g) and polyvinylidine fluoride (PVDF) binder (0.01 g) in a weight ratio of 80 : 10 : 10 in N-methyl-2-pyrrolidone (NMP) solution. The obtained slurry was coated on the Cu foil and dried in vacuum drying oven at 80 °C for 1 h to remove solution. Subsequently, the Cu foil with the active materials were dried at 120 °C for 12 h in the same vacuum drying oven and cut into round shape strips of φ 11 mm in size. The mass loading of the active materials was controlled at 1.20 mg/cm^2. The two-electrode electrochemical cells (CR2032 coin-type) were assembled in a glove box filled with high-purity argon, in which cells were assembled using the lithium metal foil (φ 15.60 mm × 0.45 mm) as reference electrode, Celgard 2400 microporous membrane as separator, and 12–13 wt% of $LiPF_6$ in the mixture of EC, DMC, EMC (1 : 1 : 1, vol%) as electrolyte. Galvanostatic charge-discharge test was carried out by LAND (CT 2001A) battery test system in the voltage range of 0.01–3.00 V. The same electrochemical cells were also used to carry out measurements of cyclic voltammetry (CV). CV and electrochemical impedance spectroscopy (EIS) measurements were carried out using the CHI 660E. The CV curves were recorded in the voltage region of 0.01–3.00 V at scan rate of 0.2 mV/s. The impedance spectra were recorded in a frequency range of 100 kHz–0.01 Hz.

3. Results and Discussion

First of all, in accordance of the standard card as JCPDS card No. 71-0591 (Fig. 1a) the structures of Fe_7S_8@C-30, Fe_7S_8@C-40 and Fe_7S_8@C-50 were indentified accurately. Meanwhile, after the Fe_7S_8 had been removed by HCl (0.1 M), the fact that retained carbon parts of Fe_7S_8@C possessed the amorphous structure was verified (Fig. S1). It was obvious that Fe_7S_8 having the nano size was totally covered by carbon materials (Fig. 1b). On the basis of results of energy dispersive X-ray (EDX), the existences of C, Fe and S were also observed clearly (Fig. S2). These XRD, TEM and TEM-EDX results were indicative of that Fe_7S_8@C-40 composite materials formed completely. In addition, compared with the Fe_7S_8@C-30, and Fe_7S_8@C-50, the Fe_7S_8@C-40 showed the relatively tremendous dispersion features (Fig. S3).

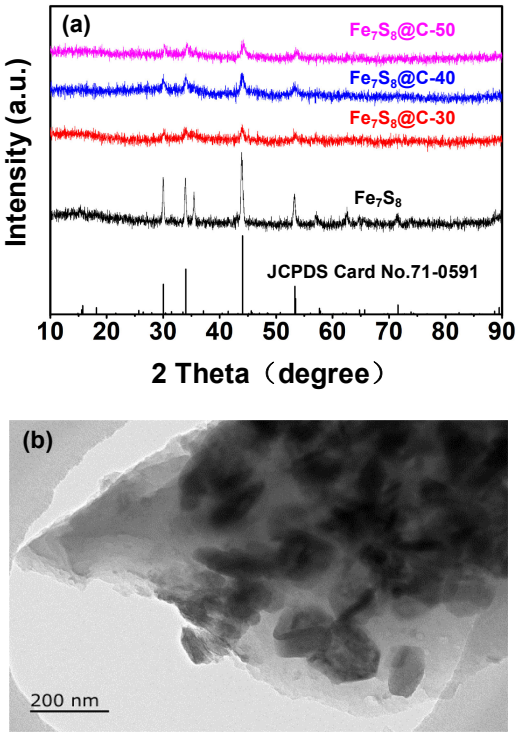

Figure 1. XRD results (a) of samples and TEM image of Fe_7S_8@C-40 (b).

It is universally acknowledged that way to cover the carbon materials on the surface of metal sulfide possesses the two important factors for storage capacity. Firstly, the conductivity of composite materials is able to improve remarkably. Secondly, the volume expansion of metal sulfide can be restricted, when the carbon materials were covered. Nevertheless, the excessive carbon materials should diminish the Li^+ storage capacity. Therefore, controlling the contents of carbon materials in composite materials is a pivotal factor in fabrications of carbon/metal sulfide composite materials.[13] The suitable carbon contents in Fe_7S_8@C materials were evaluated by the TGA evaluations. As shown in Fig. 2, the weight loss before 300 °C was naturally attributed the loss of water. The slight weight increasing was detected during the 300–400 °C, which was ascribed to the Fe_7S_8 was oxidized to the $Fe_2(SO_4)_3$. The remarkable weight loss appearing in the temperature range of 400–500 °C was considered to be the burning of the carbon materials and oxidization of Fe_7S_8. Additionally, the weight loss occurring in 500–640 °C was attributed to that Fe_7S_8 decomposed into the Fe_2O_3, SO_2 and O_2.[22] Based on the residual quantity of Fe_2O_3, the carbon contents of Fe_7S_8@C-30, Fe_7S_8@C-40 and Fe_7S_8@C-50 were calculated at 43.7%, 54.8% and 62.7%, respectively.

The conversions of surfaces and structures of Fe_7S_8@C composite materials were investigated by BET methods. As shown in Fig. S4, the Fe_7S_8@C-40 mainly possessed the microstructures at 5.9 nm which is larger than the Fe_7S_8@C-30 (3.8 nm) and Fe_7S_8@

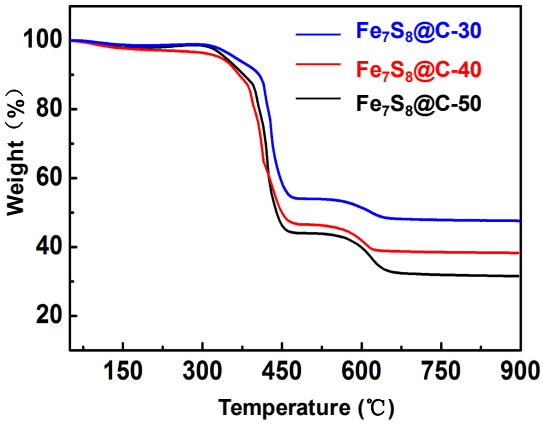

Figure 2. Thermogravimetric (TG) curves of Fe_7S_8@C composite materials.

C-50 (3.9 nm), respectively (Fig. S3). At the same time, the Fe_7S_8@C-40 also exhibited relatively bigger specific surface area than the Fe_7S_8@C-30 and Fe_7S_8@C-50 (Table S1). These mentioned above results revealed that controlling the carbon contents in Fe_7S_8@C composite materials also could converse their structures distinctly. At the present stage, we consider the comprehensive effects such as pyrolysis of gelatin and relatively excellent dispersion of Fe_7S_8 make Fe_7S_8@C-40 to have the more complex structures than the Fe_7S_8@C-30 and Fe_7S_8@C-50.

The elements on the surface of Fe_7S_8@C were investigated by the XPS measurements in detail. As shown in the Fig. 3a, it was observed that Fe, S, C, N and O elements exist on the surface of composite materials of Fe_7S_8@C. The peaks of 724.5 eV and 710.7 eV which are attributed to the Fe^{3+} were observed obviously (Fig. 3b). Meanwhile, it considered that peaks of 713.5 eV and 771.9 eV corresponded to the characteristic peaks of Fe^{2+}, and the peaks of 161.0 eV and 162.1 eV were ascribed to the S^{2-}.[14,23] In addition, the SO_x groups showed the characteristic peaks at 168.1 eV and 169.3 eV respectively (Fig. 3c).[23] On the other hand, the C1s was able to be fitted to the four peaks which are the 284.6 eV of C–C bond, 285.7 eV showing the C–N bond, 286.4 eV of C-O bond and 288.0 eV attributing to C=O bound, respectively (Fig. 3d).[24] And the peaks of 400.2 eV and 398.5 eV belonging to the N 1s were ascribed to the nitrogen elements on pyrrole or pyridine (Fig. S5). The existence of N elements could facilitate the interactions among the Fe_7S_8@C composite materials.[25]

The electrochemical performances of Fe_7S_8@C composite materials were systematically evaluated according to general methods. Figure 4a illustrated the rate performance results. After carrying out the charge-discharge 10 times at different current densities such as 0.1 A/g, 0.2 A/g, 0.5 A/g, 1.0 A/g, respectively, the Fe_7S_8@C-40 showed Li^+ storage capacity at 506.8 mAh/g when the current density recovered to the 0.1 A/g again. Similarly, the Fe_7S_8, Fe_7S_8@C-30 and Fe_7S_8@C-50 displayed the storage capacity at 211.1 mAh/g, 243.0 mAh/g, 463.3 mAh/g, respectively, after carrying the analogous rate evaluations. These results revealed that Fe_7S_8@C-40 possessed the more tremendous rate performances than Fe_7S_8, Fe_7S_8@C-30 and Fe_7S_8@C-50.

The cycling performances of C (obtained by removing the Fe_7S_8 in Fe_7S_8@C composite materials), Fe_7S_8, Fe_7S_8@C-30, Fe_7S_8@C-40 and Fe_7S_8@C-50 were measured at current density of 0.1 A/g (Fig. 4b). It was aware of that Li^+ storage capacity of C and Fe_7S_8 showed at 237.1 mAh/g and 161.1 mAh/g, respectively, after cycling the charge/discharge 100 times. The Fe_7S_8@C-30 exhibited the Li^+ storage capacity at 130.6 mAh/g, which was lower than the Fe_7S_8 and C, although the carbon materials were covered on the surface of Fe_7S_8. It led us to consider that small amount of carbon in Fe_7S_8@C composite materials could not play the role to restrict the volume expansion of Fe_7S_8, however, the relatively low storage capacity of carbon decreased the storage capacity of Fe_7S_8@C-30. On one hand, Fe_7S_8@C-40 and Fe_7S_8@C-50 manifested the Li^+ storage capacity at 638.7 mAh/g and 402.7 mAh/g, respectively, after the charge-discharge had been carried out 100 times. It is naturally considered that enhanced Li^+ storage capacity was ascribed to the markedly improved stabilities of Fe_7S_8@C-40 and Fe_7S_8@C-50, with increasing the carbon contents in Fe_7S_8@C-40 and Fe_7S_8@C-50.

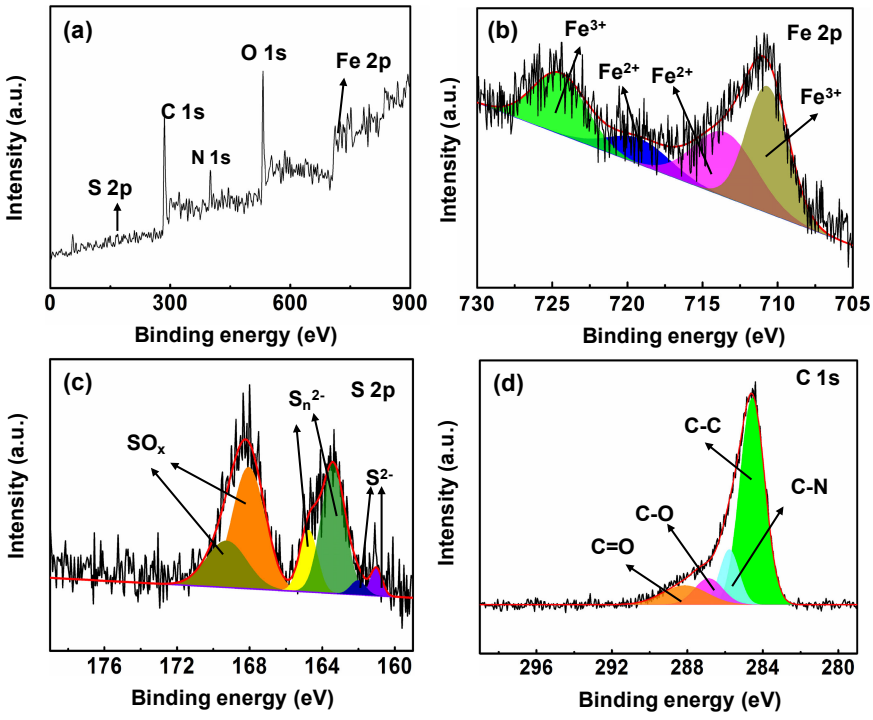

Figure 3. XPS results of Fe_7S_8@C-40.

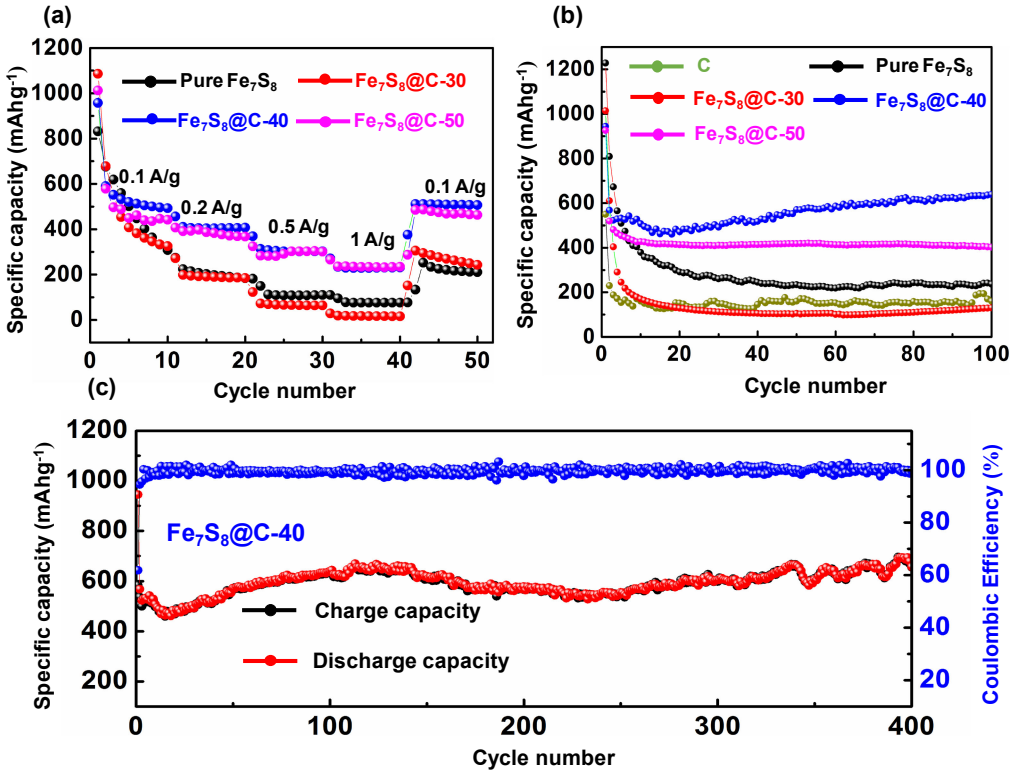

Figure 4. Rate performances (a) and cycling performances (b) of samples illustrated. (c) displays the cycling performances of Fe_7S_8@C-40, after carrying out the charge-discharge 400 times.

Furthermore, after cycling the charge-discharge 400 times, the Fe_7S_8@C-40 still showed storage capacity at 657.3 mAh/g, which indicated that Fe_7S_8@C-40 possessed the significant electrochemical stability (Fig. 4c). Meanwhile, the storage capacity of Fe_7S_8@C-40 approximately corresponds to the theoretical capacity of Fe_7S_8 showing at 663 mAh/g, which also indicates that structure of Fe_7S_8@C-40 has high stability when carrying out the Li^+ charge-discharge process.[22] Similar to reports by Wei et al., the Fe_7S_8@C-40 displayed the analogous behavior of cycling performance, leading us to consider the similar reason (explaining the behavior of cycling performance) also possibly existed in our studies.[26] Namely, the reason is probably ascribed to the influence of reversible formations of polymeric gel-like film on the surface. However, the similar cycling performance behavior was not observed in Fe_7S_8@C-50. On the other side, the similar phenomenon about the difference of cycling performance behaviors were also reported by Wang et al.[27] In this report, it was pointed out that difference was mainly attributed to the implications of carbon materials. By contrast, in our studies, associating with the BET measurement results, we conjectured that complex porous structures facilely facilitate the formation of polymeric gel-like film in Fe_7S_8@C-40, leading to it showed the different cycling performance from Fe_7S_8@C-30 and Fe_7S_8@C-50.

The charge-discharge properties of Fe_7S_8 and Fe_7S_8@C materials were displayed as shown in Fig. 5. The coulombic efficiencies of Fe_7S_8, Fe_7S_8@C-30, Fe_7S_8@C-40 and Fe_7S_8@C-50 were exhibited at 66.1%, 65.7%, 70.7% and 71.7% in first cycle, and recovered to 100% after second cycle. Basically, the coulombic efficiencies after second cycle are improved by the formation of SEI to prevent electrolyte decomposition.

Furthermore, compared with the Fe_7S_8 and Fe_7S_8@C-30, the Fe_7S_8@C-40 and Fe_7S_8@C-50 showed the excellent electrochemical stability thereby the charge-discharge plateaus were still detected after carrying out charge-discharge 100 times. Especially, considering the fact that Fe_7S_8@C-40 possessed tremendous cycling performance, the charge-discharge evaluation about the Fe_7S_8@C-40 was intentionally performed 400 times. As a result, the charge-discharge plateaus were still observed after cycling the charge-discharge 400 times, indicating the Fe_7S_8@C-40 possessed excellent electrochemical stability (Fig. 5c).

As shown in Fig. 6a–6d, the reduction potentials were observed at 0.51 V, 0.56 V, 0.61 V and 0.54 V respectively on first cycle, which were generally assigned to the formation of solid electrolyte interphase (SEI). As shown Fig. 6b–6d, according to the report by Zhou et al., the small reductive peaks of 1.61 V, 1.70 V and 1.55 V on first cycle were considered to the lithium intercalation into Fe_7S_8 to form Li_2FeS_2.[22,28] On the same first cycle, the reduction peaks attributing to $Li_2FeS_2 + 2Li^+ + 2e = 2Li_2S + Fe$ were distinctly observed at 1.09 V, 1.10 V, 1.02 V (Fig. 6b–6d).[28] Concurrently, the Fe^0 was oxidized to the Li_2FeS_2, which was respectively observed at 2.29, 1.93 and 1.95 V.[22,28] Similar to report by Zhu et al., it is also observed that small peak at 2.35 V was attributed to the formation of $Li_{2-x}FeS_2$ (Fig. 6c–6d).[19]

On the second cycle, it is obvious that above reductive peaks (0.56 V, 1.09 V and 1.61 V) of Fe_7S_8@C-30 on first cycle shifted to 0.70 V, 1.32 V and 1.54 V (Fig. 6b). Meanwhile, the reductive peaks (0.61 V, 1.10 V and 1.70 V) of Fe_7S_8@C-40 respectively shifted to 0.75 V, 1.35 V and 1.90 V (Fig. 6c), and reductive peaks (0.54 V, 1.02 V and 1.55 V) of Fe_7S_8@C-50 respectively shifted to the 0.75 V, 1.35 V and 1.90 V (Fig. 6d). Additionally, the oxidative peaks of 1.93 V and 1.95 V on first cycle shifted to the 1.97 V and 2.00 V, respectively (Fig. 6c and Fig. 6d). Similarly, the small peaks at 2.35 V also disappeared from second cycle (Fig. 6c and Fig. 6d).[19] Moreover, the oxidation-reduction peaks of Fe_7S_8@C-30 disappeared from third cycle, for the Fe_7S_8@C-30 showed instability of structure when carrying out Li^+ charge-discharge process. By contrast, the oxidation-reduction peaks of Fe_7S_8@C-40 and Fe_7S_8@C-50 still existed on third cycle. These results are also

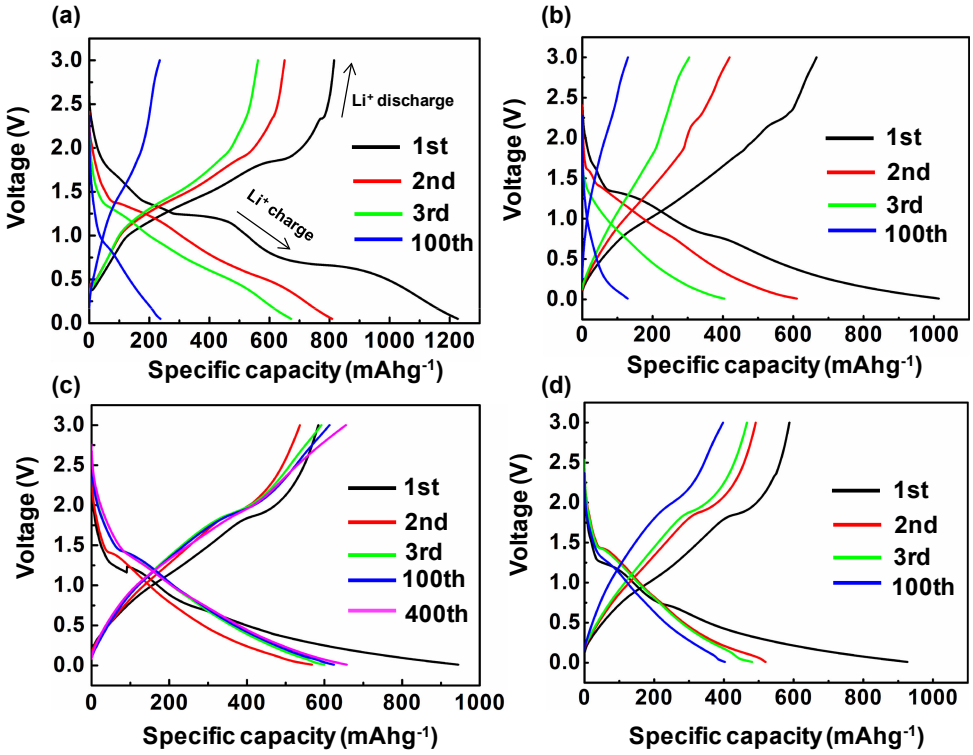

Figure 5. Charge-discharge performances of Fe_7S_8 (a), Fe_7S_8@C-30 (b), Fe_7S_8@C-40 (c) and Fe_7S_8@C-50 (d) at current density of 0.1 A/g.

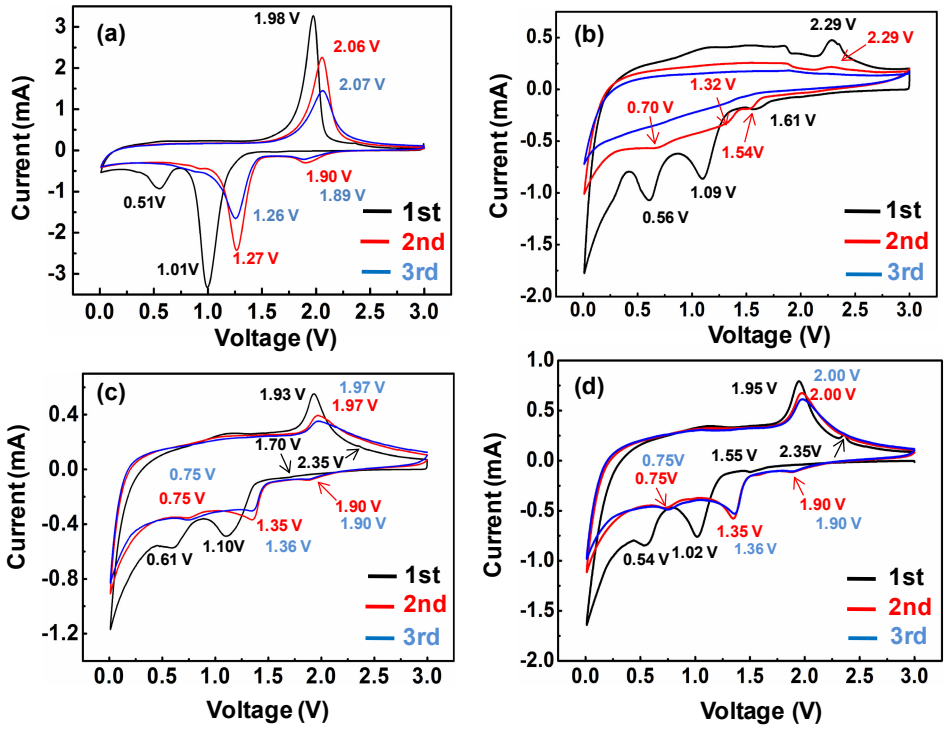

Figure 6. CV measurements of Fe_7S_8 (a), Fe_7S_8@C-30 (b), Fe_7S_8@C-40 (c) and Fe_7S_8@C-50 (d) at scan rate as 0.2 mV/s.

supportive that covering the carbon materials on surface of Fe_7S_8 helped in stability of Fe_7S_8 well.

On the other side, Fig. 7 manifested the electrochemical research-impedance results of Fe_7S_8@C composite materials. As a result, the diameter of the semicircle of negative electrodes of Fe_7S_8@C-50 were much smaller than that of Fe_7S_8, Fe_7S_8@C-30 and Fe_7S_8@C-40, which has been considerable that Fe_7S_8@C-50 electrode possesses lower charge-transfer impedances.[29,30] The more carbon contents in Fe_7S_8@C-50 caused it obviously showed more excellent conductivity than others. On one hand, the relatively high slope of Fe_7S_8@C-40 indicated it exhibited the comparatively excellent Li^+ transfer. Based on aforementioned comprehensive evaluations and associating with the rate performance measurement results, it is considered that Fe_7S_8@C-40 possessed more excellent conductive

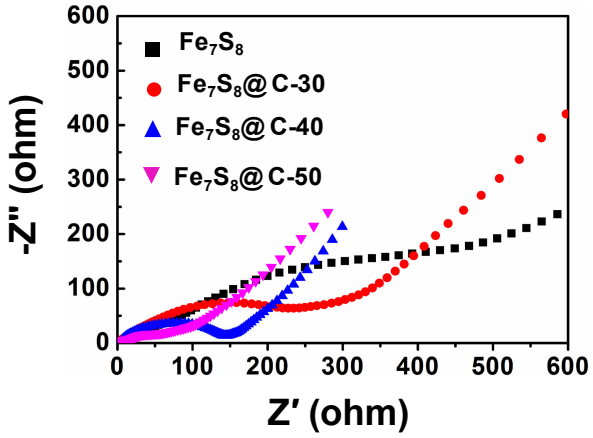

Figure 7. Nyquist plot results of Fe_7S_8@C composite materials at potential voltage around 2.1 V.

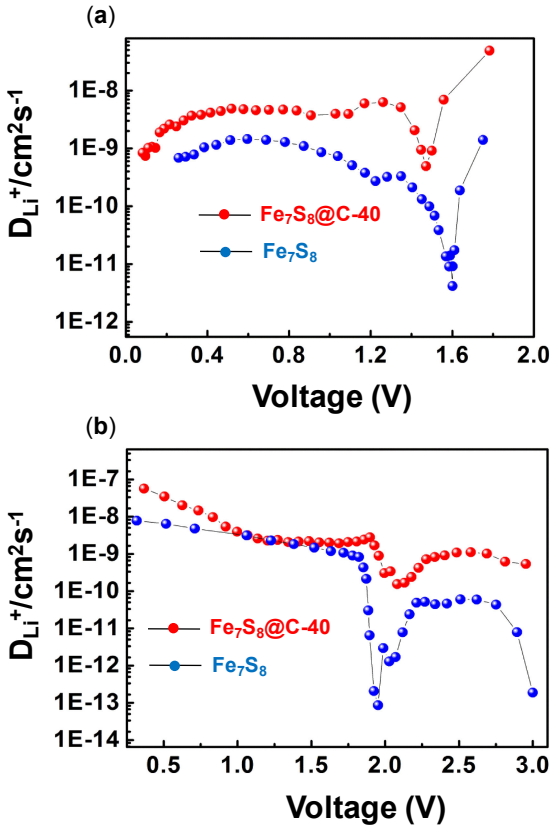

Figure 8. Relationships between voltage and D_{Li}^+ (apparent diffusion coefficients) during the discharge and charge process. (a) is the discharge process, and (b) is the charge process.

properties than others. BET results could explain the reason why Fe_7S_8@C-40 owned the excellent Li^+ transfer, for the Fe_7S_8@C-40 possessed the more complex porous structures than others (Fig. S3). Moreover, associating with the TGA results (Fig. 2), these results also led us to think of that exceedingly improved conductivity naturally linked to the suitable carbon contents in Fe_7S_8@C composite materials.

In addition, to investigate the relationships of carbon contents with the Li^+ transfer further, the galvanostatic intermittent titration technique (GITT) measurements were performed in detail.[31,32] As shown in Fig. 8(a) and Fig. 8(b), the Fe_7S_8@C-40 showed the higher Li^+ ion transfer than the Fe_7S_8 in discharge and charge processes (Fig. S6). At the present stage, we infer the significant improvement of Li^+ ions diffusion was mainly ascribed to the two factors as following. Firstly, the fact that Fe_7S_8 dispersed in carbon materials with nanometer size facilitated that Li^+ ions diffused into Fe_7S_8 lattices facilely.[19] Secondly, the markedly increased conductivity by covered carbon materials is also able to accelerate the Li^+ ions diffusion.

4. Conclusions

The Fe_7S_8@C composite materials were successfully prepared using the gelatin as carbon source, $FeSO_4{\cdot}7H_2O$ as iron source and $Na_2S{\cdot}9H_2O$ as sulfur source. This method provides the referred way to effectively prepare the Fe_7S_8@C composite materials. Compared with the Fe_7S_8, the Fe_7S_8@C-40 composite materials showed more fabulous Li^+ storage capacity, which is 657.3 mAh/g after cycling charge-discharge 400 times. It is observed that controlling the carbon contents in Fe_7S_8@C composite materials is an important factor to upgrade the Li^+ storage capacity. The possibility of Fe_7S_8 as negative electrode materials in actual fabrication of LIBs is unveiled through our studies.

Supporting Information

The Supporting Information is available on the website at DOI: https://doi.org/10.5796/electrochemistry.20-64066.

Acknowledgments

We are grateful to the support of University of Science and Technology Liaoning (601009816-39) and 2017RC03. This work was partly supported by project supported by the National Natural Science Foundation of China (Grant No. 51672117 and 51672118).

References

1. T. Kim, W. T. Song, D. Y. Son, L. K. Ono, and Y. B. Qi, *J. Mater. Chem. A*, **7**, 2942 (2019).
2. K. Wang, D. J. Ju, G. Y. Xu, B. B. Han, Y. F. Wang, J. Zhang, M. R. Chai, S. B. Chen, and W. M. Zhou, *Electrochemistry*, **88**, 8 (2020).
3. A. Prasath, A. S. Sharma, and P. Elumalai, *Ionics*, **25**, 1015 (2019).
4. T. Seko, H. Nara, M. Jeong, T. Yokoshima, T. Momma, and T. Osaka, *Electrochim. Acta*, **243**, 65 (2017).
5. W. Li, X. X. Feng, and Y. Chen, *New J. Chem.*, **43**, 14609 (2019).
6. C. C. Chang, L. C. Chen, T. Y. Hung, Y. F. Su, H. K. Su, J. H. Lin, C. W. Hu, L. Saravanan, and T. Y. Chen, *Int. J. Electrochem. Sci.*, **13**, 11762 (2018).
7. L. M. Chang, L. M. Wang, Z. M. Wang, Z. Yi, and Y. Cheng, *New J. Chem.*, **42**, 11525 (2018).
8. J. Qin, N. Q. Zhao, C. S. Shi, E. Z. Liu, F. He, L. Y. Ma, Q. Y. Li, J. J. Li, and C. N. He, *J. Mater. Chem. A*, **5**, 10946 (2017).
9. X. Y. Han, R. Li, S. Q. Qiu, X. F. Zhang, Q. Zhang, and Y. K. Yang, *RSC Adv.*, **9**, 5942 (2019).
10. K. Z. Cao, T. Jin, L. Yang, and L. F. Jiao, *Mater. Chem. Front.*, **1**, 2213 (2017).
11. Z. Yang, D. Y. Su, J. P. Yang, and J. Wang, *J. Power Sources*, **363**, 161 (2017).
12. J. K. Hu, C. F. Sun, E. Gillette, Z. Gui, Y. H. Wang, and S. B. Lee, *Nanoscale*, **8**, 12958 (2016).
13. K. Wang, D. Y. Ju, G. Y. Xu, Y. F. Wang, S. B. Chen, J. Zhang, Y. Y. Wu, and W. M. Zhou, *Int. J. Hydrogen Energy*, **44**, 25199 (2019).
14. S. C. Chen, Z. X. Kang, X. D. Zhang, J. F. Xie, H. Wang, W. Shao, X. S. Zheng, W. S. Yan, B. C. Pan, and Y. Xie, *ACS Cent. Sci.*, **3**, 1221 (2017).
15. Q. B. Zhang, J. Liao, M. Liao, J. Y. Dai, H. L. Ge, T. Duan, and W. T. Yao, *Appl. Surf. Sci.*, **473**, 799 (2019).
16. X. H. Rui, H. T. Tan, and Q. Y. Yan, *Nanoscale*, **6**, 9889 (2014).
17. X. Wei, W. H. Li, J. A. Shi, L. Gu, and Y. Yu, *ACS Appl. Mater. Interfaces*, **7**, 27804 (2015).
18. Z. Hu, Z. Q. Zhu, F. Y. Cheng, K. Zhang, J. B. Wang, C. C. Chen, and J. Chen, *Energy Environ. Sci.*, **8**, 1309 (2015).
19. L. D. Shi, D. Z. Li, J. L. Yu, H. C. Liu, Y. Zhao, H. L. Xin, Y. M. Lin, C. D. Lin, C. H. Lia, and C. Z. Zhu, *J. Mater. Chem. A*, **6**, 7967 (2018).
20. Z. Schnepp, S. C. Wimbush, M. Antonietti, and C. Giordano, *Chem. Mater.*, **22**, 5340 (2010).
21. F. Wu, R. Huang, D. B. Mu, B. R. Wu, and S. Chen, *ACS Appl. Mater. Interfaces*,

6, 19254 (2014).
22. K. L. Zhang, T. W. Zhang, J. W. Liang, Y. C. Zhu, N. Lin, and Y. T. Qian, *RSC Adv.*, **5**, 14828 (2015).
23. S. Y. Lee and Y. C. Kang, *Chem. Eur. J.*, **22**, 2769 (2016).
24. B. H. Hou, Y. Y. Wang, J. Z. Guo, Q. L. Ning, X. T. Xi, W. L. Pang, A. M. Cao, X. Wang, J. P. Zhang, and X. L. Wu, *Nanoscale*, **10**, 9218 (2018).
25. A. K. Haridas, J. Heo, Y. Liu, H. J. Ahn, X. H. Zhao, Z. Deng, M. Agostini, A. Matic, K. K. Cho, and J. H. Ahn, *ACS Appl. Mater. Interfaces*, **11**, 29924 (2019).
26. J. B. Wang, Z. W. Liu, W. J. Yang, L. J. Han, and M. D. Wei, *Chem. Commun.*, **54**, 7346 (2018).
27. Y. T. Zuo, G. Wang, J. Peng, G. Li, Y. Q. Ma, F. Yu, B. Dai, X. H. Guo, and C. P. Wong, *J. Mater. Chem. A*, **4**, 2453 (2016).
28. F. Y. Jiang, Q. Wang, R. Du, X. S. Yan, and Y. L. Zhou, *Chem. Phys. Lett.*, **706**, 273 (2018).
29. X. M. Lou, C. F. Lin, Q. Luo, J. B. Zhao, B. Wang, J. B. Li, Q. Shao, X. K. Guo, N. Wang, and Z. H. Guo, *ChemElectroChem*, **4**, 3171 (2017).
30. C. F. Lin, L. Hu, C. B. Cheng, K. Sun, X. K. Guo, Q. Shao, J. B. Li, N. Wang, and Z. H. Guo, *Electrochim. Acta*, **260**, 65 (2018).
31. G. Z. Fang, Z. X. Wu, J. Zhou, C. Y. Zhu, X. X. Cao, T. Q. Lin, Y. M. Chen, C. Wang, A. Q. Pan, and S. Q. Liang, *Adv. Energy Mater.*, **8**, 1703155 (2018).
32. Y. J. Zhang, X. Li, P. Dong, G. Wu, J. Xiao, X. Y. Zeng, Y. J. Zhang, and X. L. Sun, *ACS Appl. Mater. Interfaces*, **10**, 42796 (2018).